

1 **A novel tubulin binding molecule drives** 2 **differentiation of acute myeloid leukaemia cells**

3 Thomas R. Jackson^{1†}, Aini Vuorinen^{1†}, Laia Josa-Culleré^{2†}, Katrina S. Madden^{2,8}, Daniel Conole³,
4 Thomas J. Cogswell⁴, Isabel V. L. Wilkinson², Laura M. Kettle⁵, Douzi Zhang¹, Alison O'Mahony⁶,
5 Deanne Gracias¹, Lorna McCall⁷, Robert Westwood⁷, Georg C. Terstappen^{7,9}, Stephen G. Davies²,
6 Edward W. Tate³, Graham M. Wynne^{2,7}, Paresh Vyas^{1*}, Angela J. Russell^{2,4*}, Thomas A. Milne^{1*}

7 ¹ MRC Molecular Haematology Unit, MRC Weatherall Institute of Molecular Medicine, NIHR Oxford
8 Biomedical Research Centre Haematology Theme, Radcliffe Department of Medicine, University of
9 Oxford, Oxford, UK.

10 ² Department of Chemistry, Chemistry Research Laboratory, University of Oxford, Mansfield Road,
11 Oxford, OX1 3TA, UK.

12 ³ Department of Chemistry, Molecular Sciences Research Hub, Imperial College London, 82 Wood
13 Lane, London W12 0BZ, UK

14 ⁴ Department of Pharmacology, University of Oxford, Mansfield Road, OX1 3QT, UK.

15 ⁵ Axis Bioservices, 189 Castleroe Rd, Coleraine, Co. Londonderry, Northern Ireland BT51 3RP

16 ⁶ Eurofins Discovery Phenotypic Services, St. Charles, MO 63304 and Burlingame, CA 94010, USA

17 ⁷ Oxstem Ltd, Midland House West Way, Botley, Oxford, England, OX2 0PH

18 ⁸ Currently: School of Natural and Environmental Sciences, Newcastle University, Bedson Building,
19 Newcastle upon Tyne NE1 7RU, UK

20 ⁹ Currently: Cambrian Biopharma, New York, NY, USA

21 †These authors contributed equally to this work.

22

23 *To whom correspondence should be addressed:

24 paresh.vyas@imm.ox.ac.uk,

25 angela.russell@chem.ox.ac.uk

26 thomas.milne@imm.ox.ac.uk

27 **Abstract**

28 Acute Myeloid Leukaemia (AML) continues to have a poor prognosis, especially in the elderly. One
29 reason for this is that many treatment regimens are not well tolerated by elderly patients. Much
30 current focus is on the development of therapies that can target specific vulnerabilities of AML while
31 having fewer toxic side effects. However, despite much recent progress in developing better drugs,
32 many patients with AML still die within a year of diagnosis, partly due to the fact that it is difficult to
33 identify therapeutic targets that are effective across multiple AML subtypes. One common factor
34 across AML subtypes is the presence of a block in differentiation. Thus screening for compounds that
35 can overcome this block in genetically diverse AML models should allow for the identification of
36 agents that are not dependent on a specific mutation for their efficacy. Here, we used a phenotypic
37 screen to identify novel compounds that stimulate differentiation in several AML cell lines. Lead
38 compounds were shown to decrease tumour burden and to increase survival *in vivo*. Using multiple
39 complementary target deconvolution approaches, these compounds were revealed to be anti-
40 mitotic tubulin disruptors that cause differentiation by inducing a G2-M mitotic arrest. Together,
41 these results reveal a novel function for tubulin disruptors in causing differentiation of AML cells.

42

43 Introduction

44 Acute Myeloid Leukaemia (AML) is a haematological malignancy with around 3,000 new cases per
45 year in the UK ¹ and about 21,000 new cases per year in the US ². AML has a very poor survival rate,
46 especially in elderly patients (5-year survival less than 11% ³) which represent the majority of cases ¹.
47 The current standard of care involves inducing remission using intensive chemotherapy, such as
48 cytarabine in combination with anthracycline-derived antibiotics such as daunorubicin, followed by
49 consolidation chemotherapy or bone marrow transplantation ³⁻⁵. Such therapies are not well
50 tolerated by elderly patients and often have extensive side effects ³.

51 The promise of precision medicine is to develop targeted therapies that can specifically impact
52 cancer cells while leaving normal cells unharmed, with the hope that such therapies will be effective
53 and also have fewer toxic side effects. Characterization of a patient's underlying mutational profile is
54 becoming increasingly important for identifying patient subgroups that will be sensitive to specific
55 targeted therapies. For example, patients that carry mutations in genes such as *fms like tyrosine*
56 *kinase 3 (FLT3)* or *isocitrate dehydrogenase 1 or 2 (IDH1/2)* can be treated with small molecules
57 designed to specifically target these mutations ^{6,7}. However, due to the high levels of heterogeneity
58 among AML patients ⁸, even with patients carrying the same driver mutation, often only a subset of
59 patients respond well to targeted therapy, such as in the case of *IDH2* mutations and the drug
60 enasidenib ⁹⁻¹². In general, despite their promise, there has been a high degree of failure in clinical
61 trials for AML which utilise among novel targeted therapies ¹³.

62 Another issue with targeted therapies is that many of them benefit small patient populations only,
63 leaving the wide range of AML patients without effective treatments ¹³. The promise of
64 immunotherapies ¹⁴ and recent exciting clinical trials with the B-cell lymphoma 2 (BCL-2) inhibitor
65 venetoclax ^{3,15-17} represent two approaches for targeting AML not limited to specific mutations. Even
66 with these promising new areas of treatment, there remain patients who do not respond well to
67 treatment, and much work is being done on possible combination therapies although this is often

68 developed empirically without clear underlying mechanistic principles guiding the process³. In all,
69 there continues to be an urgent unmet need for new, well-tolerated therapies that can provide
70 complete durable remission, especially for patient subsets that do not have a clear, well defined
71 molecular target underlying the malignancy^{3, 13, 18}.

72 A defining hallmark of AML is a block in the normal myeloid differentiation process, blocking the
73 production of downstream blood lineages and disrupting normal haematopoiesis. An exciting new
74 paradigm in AML treatment is the possibility of inducing normal differentiation of AML cells by
75 removing the differentiation block. Such therapies could be both more effective and less toxic than
76 conventional chemotherapies, and may also provide effective partners for novel combination
77 therapies. As an exemplar of such an approach, a breakthrough in differentiation therapy was
78 achieved in the treatment of acute promyelocytic leukaemia (APL), which represents subset of about
79 10% of all AML patients^{19, 20}. APL is defined by a specific translocation involving the retinoic acid
80 receptor to create a fusion oncoprotein^{21, 22} which initially correlated with a poor prognosis. APL is
81 now treatable with an 85% 5-year survival rate²³ due to the introduction of differentiation therapy
82 with all-trans retinoic acid (ATRA); in combination with arsenic trioxide, a compound that causes
83 degradation of the PML-retinoic acid receptor alpha oncogenic driver fusion protein²⁴. However, this
84 therapy targets the specific oncoprotein which represents a vulnerability of APL not found in other
85 AML subsets. Nonetheless, the success of this treatment suggests that the induction of
86 differentiation by other mechanisms could provide novel treatments or new combination therapies
87 for other subtypes of AML. Indeed, when AML patients carrying *IDH1/2* neomorphic mutations
88 (mIDH, 15-25%) respond to treatment with the specific inhibitors ivosidenib (which targets mIDH1
89²⁵), or enasidenib (which targets mIDH2²⁶), they often display evidence of differentiation^{27, 28}.

90 These examples suggest that inducing differentiation in AML may be more effective than current
91 treatments. However, in each of these examples, the drugs have been developed for highly specific
92 targets which are not present in the majority of leukaemia patients. Recent work using an *in vitro*

93 screening approach to identify novel inducers of differentiation resulted in the identification of a
94 new class of dihydroorotate dehydrogenase (DHODH) inhibitors. In early preclinical work, DHODH
95 inhibitors appear to be effective at inducing differentiation in AML cells in a non-mutation specific
96 manner²⁹⁻³¹. Although it remains unclear how DHODH inhibition directly induces differentiation in
97 AML cells³¹, this work provides a promising proof of principle that such screening approaches are an
98 effective way of finding novel compounds for differentiation therapy. However, until the mechanism
99 of action of such compounds is better understood, it is unclear exactly which patient subsets will
100 respond to such a therapy, which could be part of the reason why recent clinical trials for a DHODH
101 inhibitor were terminated due to lack of benefit²⁹. Thus, there remains a further need for the
102 identification of novel compounds and alternative mechanisms that can induce differentiation in
103 AML cells in a mutation agnostic manner.

104 Here, we developed an *in vitro* flow cytometry-based phenotypic screen to identify new classes of
105 small molecules which are capable of promoting differentiation in AML blasts, and validated their
106 differentiation profiles using RNA-seq. As AML is a highly heterogeneous disease³², the phenotypic
107 screen was performed using several AML cell lines to identify molecules whose efficacy was not
108 limited to a particular genetic subtype. From the confirmed hits thus identified, a number of
109 compound series were selected for further optimisation. The resulting compounds showed *in vivo*
110 efficacy in reducing tumour burden in a subcutaneous model and displayed increased survival
111 following oral dosing in an orthotopic xenograft model. Using a combination of RNA-seq, BioMAP
112 analysis (an *in vitro* platform which uses primary human cells to test drug efficacy and toxicity) and
113 chemoproteomics, tubulin beta chain was identified as a direct binding target of these compounds.
114 Using other known, and structurally distinct tubulin binders, we showed that tubulin disruption
115 causes mitotic arrest, and mitotic arrest results in initiation of differentiation, thus highlighting a
116 novel mechanism of action and usage for the compounds we have identified.

117 **Results**

118 **A phenotypic screen for differentiation in multiple AML cell lines identifies novel compounds**

119 A screen was initiated using a library containing 1000 structurally-diverse, commercially available
120 small molecules, in order to identify compounds that were capable of differentiating four AML cell
121 lines (HL-60, OCI-AML3, THP-1, KG-1). Properties of these cell lines are summarised in Table 1, and
122 together they represent approximately 30% of known AML mutations³². CD11b is a known cell
123 surface marker of differentiated myeloid cells^{33, 34} and flow cytometry (FACs) analysis was used to
124 quantify upregulation of CD11b expression after compound treatment. As positive controls, phorbol
125 12-myristate 13-acetate (PMA³⁵) was used to induce the differentiation of HL-60 and KG-1 (Fig. 1A,
126 Supplementary Fig. 1), while tranilcypromine (TCP³⁶) was used as a positive control for THP-1 cells
127 (Supplementary Fig. 1) and GS87 was used as a positive control for OCI-AML3 cells. Cells were
128 treated with 10 μ M of compound for 4 days. Compounds that upregulated CD11b more than 10% in
129 at least 3 cell lines were considered potential hits and selected for further investigation. Using this
130 criterion, we identified 44 positive hits (Fig. 1B, Supplementary Fig. 1). The structure and CD11b
131 upregulation data of an example hit, OXS000275 **1**, is shown in Fig. 1C-D.

132 **Novel identified compounds induce both neutrophil and macrophage differentiation in an AML** 133 **cell line**

134 Concentration-dependent responses were confirmed for hit compounds such as OXS000275, which
135 was found to have a calculated EC₅₀ of 240 \pm 6 nM (Fig. 1D-E). Further effects of hit compounds on
136 cell proliferation and viability were measured by staining for dead cells with DAPI and using acridine
137 orange as a counterstain for all cells (Fig. 1F). Differentiation was also validated using morphology as
138 characterised by Wright-Giemsa staining, with lighter cytoplasm, a higher cytoplasm to nuclei ratio
139 and an increase in granulation used as signs of differentiation towards a macrophage phenotype
140 (Fig. 1G). OXS000275 significantly inhibited cell proliferation and reduced cell viability (Fig. 1F) as

141 well as promoting a morphology consistent with differentiation in all four of the cell lines (Fig. 1G,
142 Supplementary Fig. 2).

143 To further confirm that the hits were inducing differentiation, selected compounds were further
144 investigated using RNA-seq analysis, with PMA treatment used as a positive control for
145 differentiation in HL-60 cells. Both PMA and OXS000275 caused genome wide changes in gene
146 expression after 72 hours (Fig. 2A), but hierarchical clustering of genes showed that OXS000275 and
147 PMA clustered separately from each other and from the DMSO control, demonstrating OXS000275
148 and PMA caused distinct gene expression profiles (Fig. 2B). However, there is a significant overlap
149 between gene expression changes caused by OXS000275 and PMA, suggesting they both modulate
150 common biological processes (Fig. 2B and C). Using principal component analysis (PCA), compound-
151 treated HL-60 cells were compared to primary human cells of the myeloid lineage³⁷ (Fig. 2D). As
152 expected, HL-60s treated with DMSO were found to cluster closer to stem and progenitor cell
153 populations whereas cells treated with PMA and OXS000275 clustered closer to terminally
154 differentiated monocyte populations (Fig. 2D). RNA-seq signatures were also analysed using EnrichR
155 with ARCHS4 signatures, and both PMA and OXS000275 upregulated genes significantly overlapped
156 with those of macrophages, but not stem or progenitor cells (Fig. 2E). Despite PMA inducing a larger
157 number of differentially expressed genes, the macrophage signature in PMA treated cells was found
158 to be less significant and produced a lower enrichment score than in OXS000275 treated cells (Fig.
159 2E). This result potentially reflects the promiscuity of PMA and its subsequent impact on a wide
160 range of different biological processes. Besides producing a more specific macrophage signature
161 compared to PMA, OXS000275 treatment also produced a significant neutrophil gene expression
162 profile while PMA had little effect on the expression of neutrophil specific genes (Fig. 2E). Finally,
163 gene set enrichment analysis (GSEA) analysis confirmed both PMA and OXS000275 signatures were
164 enriched for macrophage genes, while OXS000275 was found to also be enriched for genes
165 associated with neutrophils whereas PMA was not (Fig. 2F). Taken together these data suggested
166 OXS000275 is able to induce global gene expression changes associated with differentiation at least

167 to the same extent as PMA treatment. However, gene expression changes induced by OXS000275
168 treatment appeared to be more specific to differentiation than those induced by PMA. Finally, unlike
169 PMA, OXS000275 treatment was able to induce upregulation of both macrophage and neutrophil
170 associated RNA signatures. A summary of EnrichR analysis of other confirmed hits from the
171 phenotypic screen can be found in Supplementary Table 1.

172 **Development of Lead Compounds**

173 Starting from confirmed hits, further optimisation afforded the lead compounds OXS007417 **2** and
174 OXS007464 **3**, both of which had higher potency and improved ADME properties relative to the
175 starting compound (Fig. 3A and B, detailed chemistry in ³⁸). We confirmed that both OXS007417 **2**
176 and OXS007464 **3** also caused differentiation of AML cell lines by showing that they upregulated
177 CD11b cell surface expression in HL-60 cells with comparable EC₅₀ values of 57 ± 3 nM and 36 ± 1 nM
178 respectively (Fig. 3B). Differentiation was further confirmed by morphology as previously described
179 (Fig. 3C).

180 **Lead Compounds Demonstrate Anti-leukaemia Activity *In Vivo* in a subcutaneous Xenograft Model** 181 **of AML**

182 To study the ability of OXS007417 **2** and OXS007464 **3** to inhibit tumour growth *in vivo*, a
183 subcutaneous xenograft model was used in the first instance and compared to standard
184 chemotherapeutic agents. HL-60 cells were implanted into the flank of female NOD SCID mice, and
185 tumours were allowed to reach a volume of 150 mm³ before commencement of treatment (Fig. 4A).
186 OXS007417 and OXS007464 were administered per os (PO) twice daily for 4 weeks at 10 and 3
187 mg/kg respectively, while cytarabine (araC) was used as a reference of the standard of care (SoC) for
188 AML ³ and administered via intraperitoneal (IP) injection, 20 mg/kg once daily ³⁹. Finally, ATRA (PO, 5
189 mg/kg 5 on/2 off) was used as reference differentiating agent. Treatments are summarised in Fig. 4A
190 and Table 2.

191 Treatment with OXS007417 was well-tolerated and did not lead to significant body weight loss in the
192 animals (Supplementary Fig. 3). After 28 days of dosing, OXS007417 significantly delayed the growth
193 of HL-60 tumours, with a tumour control ratio (T/C) of 55%, when compared to vehicle group
194 ($p < 0.0001$), (Fig. 4C and D).

195 The standard of care araC showed a less pronounced effect, with T/C of 70% ($p < 0.0001$). The
196 smallest effect was observed in the group treated with ATRA, which did not show a significant ($p =$
197 0.07) reduction of tumour volume.

198 At conclusion of the study, plasma and tumour samples were taken for bioanalysis. In animals
199 treated with OXS007417, compound exposure was detected in both samples, at 6.84×10^{-7} M (252
200 ng/mL plasma) and 2.41×10^{-9} mol/g (888 ng/g tumour) respectively. In animals treated with
201 OXS007464, compound exposure was detected in both samples, at 3.38×10^{-7} M (152 ng/mL plasma)
202 and 4.89×10^{-10} mol/g (220 ng/g tumour) respectively. OXS007464 was not as well-tolerated as
203 OXS007417 and the dosage had to be reduced with some mice showing weight loss (Supplementary
204 Fig. 3) and was therefore not used in further *in vivo* studies. The reason for this differing tolerance is
205 unclear.

206 **OXS007417 causes increased survival using an *in vivo* murine orthotopic Xenograft Model of AML**

207 Having shown *in vitro* to *in vivo* correlation using the subcutaneous HL-60 based model, the anti-
208 leukaemia activity of OXS007417 was also evaluated in an orthotopic AML model. HL-60 cells were
209 injected into the tail vein of female NCG mice, and 7 days were allowed for engraftment. Animals
210 were then dosed with OXS007417 bid (formulated in 5% DMSO : 0.1% Tween 20 in PBS; PO; 10
211 mg/kg, with a dosing volume of 10 ml/kg) for 3 weeks (Fig. 4B). Significantly, OXS007417 produced
212 prolonged survival ($p < 0.0001$) compared with the vehicle control group (Fig. 4E).

213 **Analysis from the BioMAP Phenotypic Platform suggests tubulin disruption as a MoA for** 214 **OXS007417 and OXS007464**

215 With compounds in hand displaying *in vitro* differentiation properties and *in vivo* efficacy in two
216 different tumour models, we next set out to identify the biological targets of the compounds and to
217 identify possible mechanisms of action (MoA) for their activity. The Diversity PLUS panel (BioMAP®,
218 Eurofins Discovery) is an *in vitro* platform which uses different primary human cell types to generate
219 activity profiles designed to aid MoA studies and the identification of off-target effects as well as
220 potential toxicity issues. The method utilises 12 primary cell-based systems modeling a broad scope
221 of human tissue and disease biology and 148 protein biomarkers to create a “biomarker signature
222 profile” that can be compared to a database of mechanistic signatures for >4600 compounds with
223 known MoAs. The BioMAP study found OXS007417 and OXS007464 to be anti-proliferative to
224 human primary B, T cells, coronary artery smooth muscle cells, endothelial cells, and fibroblasts (Fig.
225 5A), but not cytotoxic at the four concentrations tested (12 – 800 nM). Comparing the biological
226 activities of OXS007417 and OXS007464 to those of known bioactive agents in the BioMAP reference
227 database, OXS007417 and OXS007464 were found to have profiles most similar to microtubule
228 disruptors (Table 3 and 4).

229 **Analysis by early RNA-seq suggests tubulin disruption as a MoA for OXS007417 and OXS007464**

230 To further investigate the MoA of our novel compounds, HL-60 cells were treated for 6 hours with
231 OXS007417 **2** (1 µM), OXS007464 **3** (1 µM), PMA (10 nM) or DMSO control before global gene
232 expression changes were assessed by RNA-seq (Fig. 5 B-E). Even at this early time point, OXS007417,
233 OXS007464 and PMA induced genome wide changes in gene expression (Fig. 5 B-D).

234 As with OXS000275, hierarchical clustering of genes showed that both OXS007417 and OXS007464
235 had distinct gene expression profiles from PMA and DMSO vehicle control (Fig. 5D). Significant
236 overlap of differentially expressed genes with PMA again suggested the activation of common
237 biological processes (Fig. 5C). Although forming their own distinct clusters, OXS007417 and
238 OXS007464 clustered together with very similar gene expression profiles compared to each other,
239 relative to PMA and DMSO treatment (Fig. 5D). The similarity between OXS007417 and OXS007464

240 gene signatures is further highlighted by the almost complete overlap of differentially expressed
241 genes caused by these two compounds (Fig. 5C). The similarity between OXS007417 and OXS007464
242 at this early time point suggests a common mechanism of action is shared by these two compounds.
243 The L1000CDS2 database⁴⁰ was used to search for substances that can mimic the gene expression
244 changes observed when treating HL-60 cells with PMA, OXS007417 and OXS007464. The top ranked
245 compounds are shown in Table 5. The top ranking matches for our PMA-generated signatures were
246 monopolised by signatures produced by PMA itself or ingenol 3,20-dibenzoate (also a PKC activating
247 compound). Top ranking matches of OXS007417 and OXS007464 were, however, dominated by
248 microtubule disruptors, confirming the BioMAP analysis. In addition, gene set enrichment analysis
249 (GSEA) of OXS007417 and OXS007464 gene signatures confirmed the up-regulation of macrophage
250 and neutrophil differentiation profiles at this time point (Fig. 5E).

251 **Chemoproteomics with photoaffinity-labelled probes identifies tubulin as the drug target**

252 Chemoproteomics using clickable photoaffinity labelled probes has proven to be a powerful and
253 useful method for identification of small molecules' direct target(s) within live cells⁴¹⁻⁴⁵. Particularly,
254 UV-induced covalent bond formation between a photoaffinity-labelled probe and its target(s) has
255 proven especially useful for target identification of small molecules which bind reversibly and with
256 relatively low affinity to their targets through noncovalent interactions⁴⁶. The clickable alkyne tag
257 enables the Cu(I)-catalyzed azide-alkyne cycloaddition (CuAAC) reaction with a fluorophore- or
258 biotin-azide allowing visualization and isolation of bound target(s) by pull-down experiments
259 respectively. Thus, on the basis of structure-activity relationship information of the parent
260 compound OXS007464³⁸, we devised an affinity-based protein profiling strategy to elucidate the
261 protein targets of OXS007464 through the design and synthesis of clickable photoaffinity-labelled
262 probe **4**, which retained the ability to upregulate CD11b with reasonable levels of potency ($EC_{50} =$
263 506 ± 44 nM, Fig. 6A).

264 In order to profile the ability of probe **4** to bind to proteins in cells, probe-treated HL-60 cells were
265 exposed to irradiation (365 nm) and the resulting lysates were treated with TAMRA-azide under
266 CuAAC conditions. Labelled proteins were separated by SDS-PAGE and visualized by in-gel
267 fluorescence. Probe **4** demonstrated clear concentration-dependent labelling of proteins in HL-60
268 cells (Fig. 6B). Furthermore, it was confirmed that labelling is UV-dependent (Supplementary Fig. 4).

269 Next, we wanted to distinguish therapeutically relevant target(s) from non-specific binding by
270 carrying out competition control experiments using an excess of more potent parent compounds to
271 block the binding of probe **4**. HL-60 cells were pre-treated with increasing concentrations of parent
272 compounds OXS007464 **3** and OXS008255 **5** ($EC_{50} = 1.7 \pm 0.6$ nM, Fig. 6C-D), the latter compound
273 was a result of further optimization of OXS007417. Furthermore, the competition experiment was
274 performed with known tubulin binder paclitaxel⁴⁷. Only one band (~ 50 kDa, the known molecular
275 weight of tubulin) was clearly competed away in all cases, (Fig. 6C, Supplementary Fig. 4), with
276 OXS008255 **5** showing more potent competition than paclitaxel (Fig. 6C). Additionally, pre-treatment
277 with OXS007564 **6** (Supplementary Fig. 5), a structurally similar but inactive analogue of OXS007464
278 **3**, had no influence on the binding of probe **4** up to 5 μ M (Fig. 6D), confirming the importance of the
279 50 kDa band as a relevant target.

280 To confirm the identity of the 50 kDa band and to identify other potential targets that may be less
281 abundant and not easy to identify in the gel-based assay, we next performed a proteome-wide pull-
282 down experiment. HL-60 cells were treated with probe **4** alongside DMSO vehicle and competition
283 controls consisting of OXS008255 **5** and paclitaxel. After photocrosslinking, the resulting lysates were
284 subjected to CuAAC reaction with biotinylated AzRB capture reagent (Supplementary Fig. 6)⁴⁸.
285 Bound proteins were isolated by using NeutrAvidin beads followed by on-bead digestion and
286 analysis of resulting peptides by nanoLC-MS/MS (full proteomics data available in Supplemental data
287 S1).

288 Data analysis revealed that tubulin beta chain (TUBB) was the protein most significantly enriched by
289 probe **4** when compared to DMSO vehicle (Supplementary Fig. 7). Interestingly, competition
290 experiments with OXS008255 **5** (Fig. 6E - 1 μ M and 6F - 5 μ M) highlighted the high selectivity of our
291 compounds for the tubulin beta chain. Moreover, the competition experiments with 25 μ M of
292 OXS008255 **5** (Fig. 6G) and paclitaxel (Fig. 6H) indicated tubulin beta chain and several other proteins
293 as significant, however, tubulin beta chain was the only consistent target across all four conditions.
294 The identification of tubulin beta chain was further confirmed by immunoblotting after the pull-
295 down experiment (Fig. 6I). The results clearly show concentration-dependent competition with
296 OXS008255 **5** and paclitaxel confirming tubulin beta chain as a direct target of our compounds.

297 **OXS007417 disrupts tubulin polymerisation in a cell-free system and causes metaphase arrest *in***
298 ***vitro*.**

299 Next, OXS007417 and OXS007464 were tested for their ability to inhibit polymerisation of tubulin in
300 a cell-free system. Both compounds were found to inhibit tubulin polymerisation with IC₅₀ values of
301 1.1 μ M OXS007464, and 1.7 μ M for OXS007417 (Fig. 7A). The ability of OXS007417 to disrupt the cell
302 cycle of HL-60 cells was subsequently analysed by DNA and P-H3 staining. Cell cycle analysis showed
303 OXS007417 was able to cause G2-M mitotic arrest with cell cycle profiles comparable to those
304 produced by positive control vinblastine, a known microtubule disruptor (Fig. 7B-C). Finally, mitotic
305 spindle disruption was observed by immunohistochemistry (Fig. 7D). OXS007417 was found to
306 disrupt spindle formation with spindle morphology comparable to that of vinblastine treated cells.
307 Together, these result show that using an unbiased phenotypic screen, we were able to identify a
308 novel series of compounds that induce differentiation of four AML cell lines by binding directly to
309 tubulin and causing a G2-M cell cycle arrest.

310

311

312 Discussion

313 Despite the long term need for new therapies in AML, it has only been the last few years that have
314 produced several new therapies approved for use in the clinic^{3, 49}. However, despite these exciting
315 recent advances, many of these new therapies are only able to target a subset of AML patients. In
316 addition, even when new treatments are highly successful in targeting a specific patient subset,
317 there are many individual patients who still do not respond fully to treatment. Thus, there is still a
318 need for drugs that can target patients in a mutation and subtype independent manner, preferably
319 with low toxicity either alone or in combination with other therapies. One promising new avenue of
320 research to this end is the identification of compounds such as DHODH inhibitors that can induce
321 differentiation of leukaemia cells^{31, 50}. Here, using an unbiased phenotypic screening approach, we
322 have identified a novel class of tubulin binding molecules and have revealed a novel mechanism in
323 which tubulin binding can cause a G2-M arrest and differentiation of AML cells.

324 In order to accomplish this, we used a flow cytometry based phenotypic screen with CD11b as a pan
325 marker of myeloid differentiation to identify novel compounds that could differentiate several AML
326 cell lines. Differentiation was confirmed by an arrest in cell proliferation, appearance of a
327 differentiated cell morphology and by global gene expression analysis. Thereafter, through iterative
328 rounds of optimisation of these hits, a number of lead molecules were developed from initial hits.
329 Using these compounds *in vivo*, efficacy was demonstrated in two different xenograft models.

330 The advantage of phenotypic screening is that unlike target-based approaches, a well-designed
331 phenotypic screen can directly select for compounds that have the desired cellular activity, in this
332 case differentiation of AML cells. This provides the possibility of selecting for compounds that have
333 polypharmacology as well as identifying compounds that impact desired pathways through novel
334 mechanisms. It is generally not possible to easily accomplish either of these goals with single target-
335 based approaches, as extensive knowledge of the target is a precondition of drug development.
336 Because of this, it has been argued that successful target-based approaches have often been

337 dependent on previous phenotypic screening for identification and development of first-in-class
338 compounds, and that phenotypic screening is an important complementary approach to target
339 based methods^{51, 52}.

340 However, there are several challenges of phenotypic screens including the importance of including
341 counterscreening approaches to filter out compounds which interact with undesirable, undruggable
342 or toxicity inducing targets; as well as identifying the target of a novel compound and then
343 understanding the underlying mechanism of how target engagement impacts the cell. Here, we used
344 several complementary approaches to identify the direct target of our novel compounds and to
345 ultimately decipher their mechanism of action. To accomplish this, representative lead compounds
346 were subjected to BioMAP analysis, early time point RNA-seq analysis and chemoproteomics, with
347 all three methods converging on tubulin disruption as the MoA. Furthermore, the compounds were
348 found to upregulate differentiation signatures after just 6 h treatment.

349 Tubulin inhibitors are well known drugs in cancer therapy⁵³, but as far as we know they have not
350 previously been identified as compounds that could cause differentiation of cells. More commonly,
351 disruption of tubulin is known to lead to cell death, something we also observe in our data here.
352 Exactly how a G2-M mediated arrest could lead to differentiation is not clear, but interestingly,
353 DHODH inhibitors also seem to have this dual role in promoting a choice between differentiation or
354 cell death³¹.

355 In conclusion, we have shown that phenotypic screening can be employed to identify novel
356 compounds that exhibit the desired phenotypic activity (differentiation induction) and that a variety
357 of complementary methods can be used in the context of target deconvolution to decipher their
358 mechanism of action. Further work needs to be done to identify other compounds capable of
359 causing differentiation of AML cells, as this is likely to have a long-term impact on cancer therapy,
360 especially in those areas currently lacking safe and effective treatments.

361 **Methods**

362 **Cell Culture**

363 AML cell lines were purchased from the American Type Culture Collection (ATCC;
364 <http://www.atcc.org>) or from DSMZ (<https://www.dsmz.de/>). The cells were maintained in RPMI
365 supplemented with 10% FBS and 1% *L*-Glutamine.

366 **Compound Treatment before Flow Cytometry**

367 Compound stock solutions (10 mM) were prepared in DMSO and stored at -20 °C. Serial dilutions
368 were carried out in cell medium prior to use in each experiment and final concentration of DMSO
369 was maintained at 0.1% except for final compound concentrations above 10 mM. Cells were seeded
370 at in a 96-well plate at a density of 2x10⁴ cells/well, in a 95 mL volume, then 5 mL of compound
371 solutions (x20 of desired concentration) were added. Cells were incubated for 4 days

372 **Flow Cytometry**

373 Cells were pelleted by centrifugation at 1000 rpm and suspended in 40 mL of blocking buffer (10%
374 FBS in IMDM, no phenol red), then 10 mL of anti-human CD11b/Mac-1 (555388, BD Bioscience)
375 solution (25% in blocking buffer) was added. Cells were stored in ice for 20 min. The cell suspension
376 was centrifuged, washed three times with staining buffer (1% FBS in IMDM, no phenol red), and
377 resuspended in 200 mL of staining buffer with 1 mg/mL DAPI (Sigma-Aldrich, D9542). Flow
378 cytometry was performed on an Attune NxT flow cytometer (Thermo Fisher Scientific UK) with
379 previous compensation. Data was analysed using Attune NxT software and Flow Jo (v9).

380 **Cell counts and viability assessment**

381 Solution 13 containing acridin orange and DAPI was purchased from ChemoMetec (910-3013). After
382 the appropriate cell treatment, one volume of solution 13 was added into 19 volumes of the pre-
383 mixed cell suspension, and analysed using NucleoCounter® NC-300TM (ChemoMetec).

384 **Cytospins and Modified Wright's Staining**

385 Cells were prepared in staining buffer (IMDM, no phenol red + 1% FBS) at a concentration of
386 approximately 1×10^5 cells/ml. Cytospins were made (1,000 rpm, 5 min), and the cells allowed to air-
387 dry. Cells were stained with Modified Wright's stain using a Hematek®. Stained cells were allowed to
388 air-dry and coverslips were affixed with DPX mount prior to microscopy (Sigma-Aldrich, 06522).

389 ***In Vivo* Leukaemia Analysis: Subcutaneous Model**

390 Female NOD SCID mice aged 5-7 weeks were used for the HL-60 subcutaneous models. Cells ($5 \times$
391 10^6 cells) were implanted subcutaneously in a Matrigel matrix (1:1) onto the flank of each mouse and
392 allowed to grow to the pre-specified size of 150 mm^3 . Mice were grouped randomly into treatment
393 groups based on their bodyweight to ensure even distribution. Mice were treated as indicated in
394 Table 2. Tumours were measured 3 times per week using digital callipers. The length and width of
395 the tumour were measured, and volume calculated using the following formula: volume = (length x
396 width²)/2. The tumour control ratio (T/C) was calculated in the following way: ((Mean tumour
397 volume on day 28 – mean starting volume)/ (Mean vehicle tumour volume on day 28 – mean vehicle
398 starting volume))*100. The study was terminated the end of the 28-day treatment period.

399 ***In Vivo* Leukaemia Analysis: Subcutaneous Model Ethics**

400 All protocols used in this study were approved by the Axis Bioservices Animal Welfare and Ethical
401 Review Committee, and all procedures were carried out under the guidelines of the Animal
402 (Scientific Procedures) Act 1986.

403 ***In Vivo* Leukaemia Analysis: Orthotopic Model**

404 Female NCG recipient mice 6–8 weeks of age were used for the HL-60 orthotopic model. Cells ($1 \times$
405 10^7) were introduced intravenously by tail vein injection. Cells were given 7 days to engraft before
406 commencement of treatment. Animals were then dosed with OXS007417 (PO, 10 mg/kg) for 3
407 weeks (Fig. 4B).

408 **Isolation of RNA**

409 Total RNA for the RNA-seq was isolated using QIAGEN RNeasy-Plus Mini columns as per the
410 manufacturer's instructions. RNA purity was analysed using RNA Screen Tape with a TapeStation
411 system (Agilent).

412 **RNA-Seq**

413 Poly-A containing mRNA molecules were purified from total RNA using oligo-dT attached magnetic
414 beads. Following purification, the mRNA was fragmented using divalent cations under elevated
415 temperature. First strand cDNA was synthesised using random primers (NEB). Following second
416 strand cDNA synthesis, cDNA libraries underwent end repair, a single adenylation of the 3' ends and
417 TRUE-seq adapter ligation. Libraries were enriched by PCR (15 cycles). Library quality was assessed
418 by DNA Screen Tape with Tape Station system (Agilent), quantified by Qubit assay (Thermo Fisher
419 Scientific) and pooled. Next-generation sequencing of pooled libraries was performed (Illumina
420 NextSeq), resulting in approximately 10 million pairs of 75-bp reads per sample.

421 **Gene Expression Analysis**

422 Following sequencing, QC analysis was conducted using the fastQC package
423 (<http://www.bioinformatics.babraham.ac.uk/projects/fastqc>). Reads were mapped to the human
424 genome assembly hg19 using STAR⁵⁴. The featureCounts function from the Subread package was
425 used to quantify gene expression levels using standard parameters⁵⁵. This was used to identify
426 differential gene expression globally, using the DESeq2 package⁵⁶.

427 **Analysis of Cell Cycle by Flow Cytometry.**

428 Cells were harvested at indicated time points, washed in PBS and suspended in hypotonic
429 fluorochrome solution [50 µg/ml propidium iodide (PI), 0.1% (w/v) sodium citrate, 0.1% (v/v) Triton
430 X-100] and stored for at least 1 h in the dark at 4 °C. Cells were washed in PBS and samples then
431 incubated with anti-PH3 (1:40) in FACS staining buffer (IMDM, no phenol red + 10% FBS) for 20 min

432 at 4 °C in the dark. Cells were washed in FACS buffer (IMDM, no phenol red + 1% FBS) and flow
433 cytometry was performed using an Attune NxT. Results were analysed using FlowJo_V10 software.

434 **Immunohistochemistry**

435 Cells were washed with PBS and resuspended in 100% FCS and cytopun onto coated slides using a
436 Shandon Cytospin 4 (Thermo Scientific) at 30g for 5 min. Cytospins were fixed in methanol for 7
437 minutes at -20°C and dipped 10 times in ice-cold acetone. Slides were then washed three times in
438 TBS 0.01% Tween 20 (TBST) for 5 minutes on a mechanical rocker. Cells were subsequently blocked
439 for 15 minutes at room temperature in TBS, 0.05% Tween 20, 1% bovine serum albumin (BSA).
440 Samples were covered with 50 µl of TBS, 0.025% Tween 20, 1% BSA containing anti-tubulin, overlain
441 with a cover slip and incubated overnight at 4°C in a humid chamber. Cover slips were then removed
442 and slides were washed three times for five minutes with TBST, covered with 50 µl containing the
443 appropriate secondary antibody and incubated in the dark for 40 minutes. Slides were then washed
444 three times for five minutes with TBST, and once for 2 minutes with PBS. Samples were then counter
445 stained with 0.25 µg/ml DAPI for 1 min, mounted using ProLong Gold antifade reagent (Invitrogen)
446 and imaged using a widefield fluorescence microscope (DeltaVision Elite, imsol).

447 **General protocol for treatment and lysis**

448 HL-60 cells (2×10^6 cells/mL in serum free RPMI media) were treated for 1 h with the probe **4** or
449 DMSO vehicle at 37 °C. In the case of competition experiments, cells were pre-treated with
450 competitor or DMSO vehicle for 30 min followed by 1 h treatment with probe **4**. Treated cells were
451 pelleted and washed with PBS. The resulting pellets were resuspended in PBS and irradiated at 365
452 nm for 5 min (100 W lamp, VWR 36595-021) on ice. Cells were lysed in buffer containing 0.1% SDS,
453 1% Triton -X-100 and 1× EDTA-free protease inhibitor cocktail (Calbiochem set III, 539134) in PBS.
454 Protein concentration of each lysate was determined using a BCA assay (Merck, 71285).

455 **In-gel fluorescence**

456 40 μL of each lysate (concentrations adjusted to 1 $\mu\text{g}/\mu\text{L}$) was treated with 2.4 μL of premixed click
457 chemistry mixture (final concentrations of 100 μM TAMRA- N_3 (Sigma-Aldrich, 760757), 1 mM CuSO_4 ,
458 1 mM TCEP and 100 μM TBTA) for 1 h. Proteins were precipitated using $\text{MeOH}/\text{CHCl}_3$ and the
459 resulting pellets washed twice with MeOH. The air-dried pellets were dissolved in 20 μL of 1 \times
460 NuPAGE LDS buffer with 0.1% mercaptoethanol and heated at 95 $^\circ\text{C}$ for 5 min. The proteins were
461 separated by NuPAGE 4-12% Bis-Tris gel in MES SDS running buffer. The gel was imaged using a
462 Typhoon FLA 9500 scanner and then stained with Coomassie (InstantBlueTM, Expedeon) and imaged
463 using a BioRad ChemiDoc scanner.

464 **Proteomics**

465 HL-60 cells were treated in triplicate and lysed as described above. 400 μL of each lysate
466 (concentrations adjusted to 2.5 $\mu\text{g}/\mu\text{L}$) was treated with 24 μL of a click chemistry master mix (final
467 concentrations of 100 μM AzRB, 1 mM CuSO_4 , 1 mM TCEP and 100 μM TBTA) for 1 h. The click
468 reaction was quenched by adding 8 μL of 500 mM EDTA (10 mM final concentration). Proteins were
469 precipitated using $\text{MeOH}/\text{CHCl}_3/\text{H}_2\text{O}$ and the resulting pellets washed twice with MeOH. The air-
470 dried pellets were dissolved in 80 μL of 1% SDS in 50 mM HEPES pH 8.0 by vortexing and sonicating
471 and then diluted to 400 μL with 50 mM HEPES pH 8.0 (0.2% SDS final concentration).

472 Samples were incubated with 100 μL (1:10 ratio of bead suspension:protein) of NeutrAvidin agarose
473 resin (Thermo Scientific 29201, pre-washed three times with 1 mL of 0.2% SDS in 50 mM HEPES pH
474 8.0) for 2 h at room temperature. The supernatants were removed and the beads washed three
475 times with 1mL of 0.2% SDS in 50 mM HEPES pH 8.0 and then twice with 50 mM HEPES pH 8.0. The
476 beads were then resuspended in 150 μL of 50 mM HEPES pH 8.0 and on-bead proteins were reduced
477 with TCEP (5 mM final concentration) and alkylated with CAA (15 mM final concentration) for 10 min
478 with gentle shaking. Proteins were digested overnight at 37 $^\circ\text{C}$ with 5 μL of trypsin (1 μg dissolved in
479 50 mM HEPES pH 8.0, Promega V5111). The trypsin digestion was quenched by adding 4 μL of 1 \times
480 EDTA-free protease inhibitor cocktail (Roche 11873580001). The supernatants were collected and

481 the beads washed (50 μ L) with 50 mM HEPES pH 8.0. The second wash was combined with the
482 corresponding supernatant and vacuum-dried. The peptide solutions were desalted on stage-tips
483 according to a published protocol⁵⁷. The peptides were eluted from the sorbent (Empore™ SDB-XC
484 solid phase extraction discs, 3M, 2240) with 60% acetonitrile in water (60 μ L), dried in a Savant
485 SPD1010 SpeedVac® Concentrator (Thermo Scientific) and stored at -80 °C until LC-MS/MS analysis.
486 Peptides were reconstituted in 2% acetonitrile in water with 0.5% trifluoroacetic acid for LC-MS/MS
487 analysis.

488 **NanoLC-MS/MS analysis**

489 Peptides were separated on an EASY-Spray™ Acclaim PepMap C18 column (50 cm \times 75 μ m inner
490 diameter, Thermo Fisher Scientific) using a binary solvent system of 2% acetonitrile with 0.1% formic
491 acid (Solvent A) and 80% acetonitrile with 0.1% formic acid (Solvent B) in an Easy nLC-1000 system
492 (Thermo Fisher Scientific). 2 μ L of peptide solution was loaded using Solvent A onto an Acclaim
493 PepMap100 C18 trap column (2 cm \times 75 μ m inner diameter), followed by a linear gradient
494 separation of 0-100% Solvent B over 70 mins at a flow rate of 250 nL/min. Liquid chromatography
495 was coupled to a QExactive mass spectrometer via an easy-spray source (Thermo Fisher Scientific).
496 The QExactive was operated in data-dependent mode with survey scans acquired at a resolution of
497 70,000 at m/z 200 (transient time 256 ms). Up to 10 of the most abundant isotope patterns with
498 charge +2 to +7 from the survey scan were selected with an isolation window of 2.0 m/z and
499 fragmented by HCD with normalized collision energies of 25. The maximum ion injection times for
500 the survey scan and the MS/MS scans (acquired with a resolution of 17 500 at m/z 200) were 20 and
501 120 ms, respectively. The ion target value for MS was set to 10^6 and for MS/MS to 10^5 , and the
502 intensity threshold was set to 8.3×10^2 .

503 **Proteomics database search and data analysis**

504 Processing of LC-MS/MS data was performed in MaxQuant version 1.6.6.0 using the built-in
505 Andromeda search engine. Peptides were identified from the MS/MS spectra searched against the

506 human reference proteome (Uniprot, Taxon ID: 9606, accessed 4th September 2019). Cysteine
507 carbamidomethylation was set as a fixed modification, and methionine oxidation and N-terminal
508 acetylation were set as variable modifications. 'Trypsin/P' was chosen as digestion mode enzyme.
509 Minimum peptide length was set to 7 residues and maximum 2 missed cleavages were allowed.
510 'Unique and razor peptides' were chosen for protein quantification. Quantification parameters were
511 set to 'standard' and 'LFQ'. Other parameters were used as pre-set in the software.

512 Data analysis was performed using Perseus (version 1.6.6.0). MaxQuant proteinGroups.txt output
513 files were filtered against contaminants and reverse dataset. Base 2 logarithm was applied to all
514 measurements and the median values within each sample were subtracted to normalise for sample
515 variation associated with overall protein abundance. The replicates for each condition were grouped
516 and the proteins with at least two valid values within a group were kept. A student's t-test (FDR =
517 0.05; $S_0 = 0.1$) was performed between the active probe sample and each DMSO control, and
518 between active probe sample and probe/parent competition samples. For mathematical reasons⁵⁸,
519 S_0 was kept low. The results were plotted using GraphPad Prism.

520 **Data availability**

521 Processed proteomics data are available in Supplementary tables 2-6. The raw mass spectrometry
522 proteomics files and database search results have been deposited at the ProteomeXchange
523 Consortium (<http://proteomecentral.proteomexchange.org>) via the PRIDE partner repository⁵⁹ with
524 data set identifier PXD0022038.

525 **Western blotting**

526 HL-60 cells were treated and lysed as described above. 100 μ L of each lysate (concentrations
527 adjusted to 2.5 μ g/ μ L) was treated with 6 μ L of premixed click chemistry mixture (final
528 concentrations of 100 μ M biotin- N_3 (Sigma-Aldrich, 762024), 1 mM $CuSO_4$, 1 mM TCEP and 100 μ M
529 TBTA) for 1 h. The click reactions were quenched by adding 2 μ L of 500 mM EDTA (10 mM final
530 concentration). Proteins were precipitated using $MeOH/CHCl_3/H_2O$ and the resulting pellets were

531 washed twice with MeOH. The air-dried pellets were dissolved in 80 μ L of 1% SDS in PBS by
532 vortexing and sonicating and then diluted to 400 μ L with PBS.

533 Samples were incubated with 15 μ L of MyOne™ Streptavidin T1 Dynabeads™ (Thermo Scientific,
534 29201, pre-washed three times with 0.2% SDS in PBS) for 1 h in the shaker. The supernatants were
535 removed and the beads washed three times with 0.1% SDS, 1% TritonX-100 in PBS and then three
536 times with 0.2% SDS in PBS. The beads were resuspended in 50 μ L of 1 \times NuPAGE LDS buffer with
537 0.1% mercaptoethanol and heated at 95 °C for 5 min. The eluted proteins were separated by
538 NuPAGE 4-12% Bis-Tris gel in MES SDS running buffer and transferred to a PVDF membrane (Bio-Rad,
539 162-0263). Tubulin beta chain protein was detected with an anti-TUBB antibody (1:500 in 5% fat-free
540 milk solution in TBST, Invitrogen MA5-16308) followed by an anti-mouse secondary antibody (Alexa
541 Fluor™ Plus 800, 1:10000, ThermoFisher A32730). The blots were imaged with a Licor Odyssey
542 system.

543 **Microtubule polymerisation assay**

544 The microtubule polymerisation assay was performed using porcine neuronal tubulin (Cytoskeleton,
545 Inc, BK006P) as an adaptation of the original method of Shelanski et al. and Lee et al.^{60, 61} at
546 Cytoskeleton, Inc.

547

548 **Acknowledgments**

549 T.A.M. is supported by Medical Research Council (MRC, UK) Molecular Haematology Unit grant
550 MC_UU_00016/6. T.R.J., A.V, L.J-C., T.J.C., and D.Z. and the experimental data were all supported
551 with a grant from OxStem Oncology. We'd like to acknowledge Ashley David and Robert Hom from
552 Cytoskeleton Inc (1830 S. Acoma St. Denver, CO 80223, USA) for suggestions and productive
553 discussions.

554 **Author contributions**

555 T.R.J., A.V, L.J-C., K.S.M., D.C., T.J.C., I.V.L.W., L.K., L.M., R.W., S.G.D., E.W.T., G.M.W., P.V., A.J.R. and
556 T.A.M. conceived the experimental design; T.R.J., A.V, L.J-C., K.S.M., D.C., T.J.C., I.V.L.W., L.K., D.Z.,
557 and D.G. carried out experiments; T.R.J., A.V, L.J-C. and L.K. analysed and curated the data; T.R.J.,
558 A.V, L.J-C., R.W., S.G.D., E.W.T., G.M.W., P.V., A.J.R. and T.A.M. interpreted the data; R.M., A.D.,
559 A.O'M., R.W., G.C.T. and S.G.D. provided expertise; T.R.J., A.V, L.J-C., A.J.R. and T.A.M. wrote the
560 manuscript; all authors contributed to reviewing and editing the manuscript; P.V., A.J.R. and T.A.M.
561 provided supervision and funding.

562 **Competing Interests Statement**

563 A.O'M. is an employee of Eurofins Discovery. S.G.D, P.V., A.J.R. and T.A.M. are all founding
564 shareholders of OxStem Oncology Limited (OSO), a subsidiary company of OxStem Limited. L.M.,
565 G.M.W. and G.C.T. are all former employees of OxStem. G.C.T. is a current employee of Cambrian
566 Biopharma. L.M.K. is an employee of Axis Bioservices Limited.

567

568 References

- 569 1. Cancer Research UK (<http://www.cancerresearchuk.org/cancer->
570 [info/cancerstats/types/leukaemia-aml/](http://www.cancerresearchuk.org/cancer-info/cancerstats/types/leukaemia-aml/)).
- 571 2. Siegel, R.L., Miller, K.D. & Jemal, A. Cancer statistics, 2019. *CA Cancer J Clin* **69**, 7-34 (2019).
- 572 3. Daver, N. *et al.* New directions for emerging therapies in acute myeloid leukemia: the next
573 chapter. *Blood Cancer J* **10**, 107 (2020).
- 574 4. Yates, J.W., Wallace, H.J., Jr., Ellison, R.R. & Holland, J.F. Cytosine arabinoside (NSC-63878)
575 and daunorubicin (NSC-83142) therapy in acute nonlymphocytic leukemia. *Cancer*
576 *Chemother Rep* **57**, 485-488 (1973).
- 577 5. Dombret, H. & Gardin, C. An update of current treatments for adult acute myeloid leukemia.
578 *Blood* **127**, 53-61 (2016).
- 579 6. Daver, N., Schlenk, R.F., Russell, N.H. & Levis, M.J. Targeting FLT3 mutations in AML: review
580 of current knowledge and evidence. *Leukemia* **33**, 299-312 (2019).
- 581 7. Liu, X. & Gong, Y. Isocitrate dehydrogenase inhibitors in acute myeloid leukemia. *Biomark*
582 *Res* **7**, 22 (2019).
- 583 8. Ivey, A. *et al.* Assessment of Minimal Residual Disease in Standard-Risk AML. *N Engl J Med*
584 **374**, 422-433 (2016).
- 585 9. Quek, L. *et al.* Clonal heterogeneity of acute myeloid leukemia treated with the IDH2
586 inhibitor enasidenib. *Nat Med* **24**, 1167-1177 (2018).
- 587 10. Stein, E.M. *et al.* Molecular remission and response patterns in patients with mutant-IDH2
588 acute myeloid leukemia treated with enasidenib. *Blood* **133**, 676-687 (2019).
- 589 11. Pollyea, D.A. *et al.* Enasidenib, an inhibitor of mutant IDH2 proteins, induces durable
590 remissions in older patients with newly diagnosed acute myeloid leukemia. *Leukemia* **33**,
591 2575-2584 (2019).
- 592 12. Bristol Myers Squibb (<https://news.bms.com/press-release/corporatefinancial-news/bristol->
593 [myers-squibb-provides-update-phase-3-idhidentify-trial-p](https://news.bms.com/press-release/corporatefinancial-news/bristol-myers-squibb-provides-update-phase-3-idhidentify-trial-p) 2020).
- 594 13. Cucchi, D.G.J. *et al.* Two decades of targeted therapies in acute myeloid leukemia. *Leukemia*
595 (2021).
- 596 14. Jakobsen, N.A. & Vyas, P. From genomics to targeted treatment in haematological
597 malignancies: a focus on acute myeloid leukaemia. *Clin Med (Lond)* **18**, s47-s53 (2018).
- 598 15. DiNardo, C.D. *et al.* Azacitidine and Venetoclax in Previously Untreated Acute Myeloid
599 Leukemia. *N Engl J Med* **383**, 617-629 (2020).
- 600 16. DiNardo, C.D. *et al.* Safety and preliminary efficacy of venetoclax with decitabine or
601 azacitidine in elderly patients with previously untreated acute myeloid leukaemia: a non-
602 randomised, open-label, phase 1b study. *Lancet Oncol* **19**, 216-228 (2018).
- 603 17. Killock, D. Venetoclax in AML: efficacy confirmed. *Nat Rev Clin Oncol* **17**, 592 (2020).
- 604 18. Watts, J. & Nimer, S. Recent advances in the understanding and treatment of acute myeloid
605 leukemia. *F1000Res* **7** (2018).
- 606 19. Wang, Z.Y. & Chen, Z. Acute promyelocytic leukemia: from highly fatal to highly curable.
607 *Blood* **111**, 2505-2515 (2008).
- 608 20. Tallman, M.S. & Altman, J.K. Curative strategies in acute promyelocytic leukemia.
609 *Hematology Am Soc Hematol Educ Program*, 391-399 (2008).
- 610 21. Borrow, J., Goddard, A.D., Sheer, D. & Solomon, E. Molecular Analysis of Acute
611 Promyelocytic Leukemia Breakpoint Cluster Region on Chromosome-17. *Science* **249**, 1577-
612 1580 (1990).
- 613 22. Dethe, H., Chomienne, C., Lanotte, M., Degos, L. & Dejean, A. The T(15-17) Translocation of
614 Acute Promyelocytic Leukemia Fuses the Retinoic Acid Receptor-Alpha Gene to a Novel
615 Transcribed Locus. *Nature* **347**, 558-561 (1990).
- 616 23. Coombs, C.C., Tavakkoli, M. & Tallman, M.S. Acute promyelocytic leukemia: where did we
617 start, where are we now, and the future. *Blood Cancer Journal* **5** (2015).

- 618 24. Miller, W.H., Jr., Schipper, H.M., Lee, J.S., Singer, J. & Waxman, S. Mechanisms of action of
619 arsenic trioxide. *Cancer Res* **62**, 3893-3903 (2002).
- 620 25. Dhillon, S. Ivosidenib: First Global Approval. *Drugs* **78**, 1509-1516 (2018).
- 621 26. Kim, E.S. Enasidenib: First Global Approval. *Drugs* **77**, 1705-1711 (2017).
- 622 27. Amatangelo, M.D. *et al.* Enasidenib induces acute myeloid leukemia cell differentiation to
623 promote clinical response. *Blood* **130**, 732-741 (2017).
- 624 28. DiNardo, C.D. *et al.* Durable Remissions with Ivosidenib in IDH1-Mutated Relapsed or
625 Refractory AML. *N Engl J Med* **378**, 2386-2398 (2018).
- 626 29. ClinicalTrials.gov (<https://ClinicalTrials.gov/show/NCT03404726>, 2021).
- 627 30. Sykes, D.B. *et al.* Inhibition of Dihydroorotate Dehydrogenase Overcomes Differentiation
628 Blockade in Acute Myeloid Leukemia. *Cell* **167**, 171-186 e115 (2016).
- 629 31. Christian, S. *et al.* The novel dihydroorotate dehydrogenase (DHODH) inhibitor BAY 2402234
630 triggers differentiation and is effective in the treatment of myeloid malignancies. *Leukemia*
631 **33**, 2403-2415 (2019).
- 632 32. Papaemmanuil, E. *et al.* Genomic Classification and Prognosis in Acute Myeloid Leukemia.
633 *New England Journal of Medicine* **374**, 2209-2221 (2016).
- 634 33. DiScipio, R.G., Daffern, P.J., Schraufstatter, I.U. & Sriramarao, P. Human polymorphonuclear
635 leukocytes adhere to complement factor H through an interaction that involves
636 alphaMbeta2 (CD11b/CD18). *J Immunol* **160**, 4057-4066 (1998).
- 637 34. Losse, J., Zipfel, P.F. & Jozsi, M. Factor H and factor H-related protein 1 bind to human
638 neutrophils via complement receptor 3, mediate attachment to *Candida albicans*, and
639 enhance neutrophil antimicrobial activity. *J Immunol* **184**, 912-921 (2010).
- 640 35. Lee, C.W., Sokoloski, J.A., Sartorelli, A.C. & Handschumacher, R.E. Induction of the
641 differentiation of HL-60 cells by phorbol 12-myristate 13-acetate activates a Na(+)-
642 dependent uridine-transport system. Involvement of protein kinase C. *Biochem J* **274** (Pt 1),
643 85-90 (1991).
- 644 36. Schenk, T. *et al.* Inhibition of the LSD1 (KDM1A) demethylase reactivates the all-trans-
645 retinoic acid differentiation pathway in acute myeloid leukemia. *Nat Med* **18**, 605-611
646 (2012).
- 647 37. Corces, M.R. *et al.* Lineage-specific and single-cell chromatin accessibility charts human
648 hematopoiesis and leukemia evolution. *Nat Genet* **48**, 1193-1203 (2016).
- 649 38. Josa-Culleré, L. *et al.* A phenotypic screen identifies a compound series that induces
650 differentiation of acute myeloid leukemia cells in vitro and shows anti-tumour effects in vivo.
651 *bioRxiv* (2020).
- 652 39. Altman, J.K. *et al.* Inhibition of Mnk kinase activity by cercosporamide and suppressive
653 effects on acute myeloid leukemia precursors. *Blood* **121**, 3675-3681 (2013).
- 654 40. Duan, Q. *et al.* L1000CDS(2): LINCS L1000 characteristic direction signatures search engine.
655 *NPJ Syst Biol Appl* **2** (2016).
- 656 41. Eirich, J. *et al.* Pretubulysin derived probes as novel tools for monitoring the microtubule
657 network via activity-based protein profiling and fluorescence microscopy. *Mol Biosyst* **8**,
658 2067-2075 (2012).
- 659 42. Li, W. *et al.* Chemoproteomics Reveals the Antiproliferative Potential of Parkinson's Disease
660 Kinase Inhibitor LRRK2-IN-1 by Targeting PCNA Protein. *Mol Pharm* **15**, 3252-3259 (2018).
- 661 43. Parker, C.G. *et al.* Ligand and Target Discovery by Fragment-Based Screening in Human Cells.
662 *Cell* **168**, 527-541 e529 (2017).
- 663 44. Shi, H., Zhang, C.J., Chen, G.Y. & Yao, S.Q. Cell-based proteome profiling of potential
664 dasatinib targets by use of affinity-based probes. *J Am Chem Soc* **134**, 3001-3014 (2012).
- 665 45. van Delft, M.F. *et al.* A small molecule interacts with VDAC2 to block mouse BAK-driven
666 apoptosis. *Nat Chem Biol* **15**, 1057-1066 (2019).
- 667 46. Wilkinson, I.V.L., Terstappen, G.C. & Russell, A.J. Combining experimental strategies for
668 successful target deconvolution. *Drug Discov Today* (2020).

- 669 47. Nogales, E., Wolf, S.G., Khan, I.A., Luduena, R.F. & Downing, K.H. Structure of tubulin at 6.5 Å
670 and location of the taxol-binding site. *Nature* **375**, 424-427 (1995).
- 671 48. Broncel, M. *et al.* Multifunctional reagents for quantitative proteome-wide analysis of
672 protein modification in human cells and dynamic profiling of protein lipidation during
673 vertebrate development. *Angew Chem Int Ed Engl* **54**, 5948-5951 (2015).
- 674 49. Patel, S.A. & Gerber, J.M. A User's Guide to Novel Therapies for Acute Myeloid Leukemia.
675 *Clin Lymphoma Myeloma Leuk* **20**, 277-288 (2020).
- 676 50. Sykes, D.B. The emergence of dihydroorotate dehydrogenase (DHODH) as a therapeutic
677 target in acute myeloid leukemia. *Expert Opin Ther Targets* **22**, 893-898 (2018).
- 678 51. Swinney, D.C. The contribution of mechanistic understanding to phenotypic screening for
679 first-in-class medicines. *J Biomol Screen* **18**, 1186-1192 (2013).
- 680 52. Moffat, J.G., Vincent, F., Lee, J.A., Eder, J. & Prunotto, M. Opportunities and challenges in
681 phenotypic drug discovery: an industry perspective. *Nat Rev Drug Discov* **16**, 531-543 (2017).
- 682 53. Arnst, K.E. *et al.* Current advances of tubulin inhibitors as dual acting small molecules for
683 cancer therapy. *Med Res Rev* **39**, 1398-1426 (2019).
- 684 54. Dobin, A. & Gingeras, T.R. Mapping RNA-seq Reads with STAR. *Curr Protoc Bioinformatics* **51**,
685 11.14.11-11.14.19 (2015).
- 686 55. Liao, Y., Smyth, G.K. & Shi, W. The R package Rsubread is easier, faster, cheaper and better
687 for alignment and quantification of RNA sequencing reads. *Nucleic Acids Res* **47**, e47 (2019).
- 688 56. Love, M.I., Huber, W. & Anders, S. Moderated estimation of fold change and dispersion for
689 RNA-seq data with DESeq2. *Genome Biol* **15**, 550 (2014).
- 690 57. Rappsilber, J., Ishihama, Y. & Mann, M. Stop and go extraction tips for matrix-assisted laser
691 desorption/ionization, nanoelectrospray, and LC/MS sample pretreatment in proteomics.
692 *Anal Chem* **75**, 663-670 (2003).
- 693 58. Giai Gianetto, Q., Coute, Y., Bruley, C. & Burger, T. Uses and misuses of the fudge factor in
694 quantitative discovery proteomics. *Proteomics* **16**, 1955-1960 (2016).
- 695 59. Perez-Riverol, Y. *et al.* The PRIDE database and related tools and resources in 2019:
696 improving support for quantification data. *Nucleic Acids Res* **47**, D442-D450 (2019).
- 697 60. Shelanski, M.L., Gaskin, F. & Cantor, C.R. Microtubule assembly in the absence of added
698 nucleotides. *Proc Natl Acad Sci U S A* **70**, 765-768 (1973).
- 699 61. Lee, J.C. & Timasheff, S.N. In vitro reconstitution of calf brain microtubules: effects of
700 solution variables. *Biochemistry* **16**, 1754-1764 (1977).

701

702

703 Figure Legends

704 **Figure 1: Phenotypic Screening and Validation of Primary Hits in HL-60 AML cell line.** A) Upon
705 treatment with positive control, PMA, HL-60 cells differentiate and up-regulate cell surface marker
706 CD11b as detected by flow cytometry. B) Scatter plot distribution showing the results of HL-60
707 screening of 1000 compound library. C) Example of a biologically active compound identified
708 (OXS000275 **1**). D) OXS000275 up-regulated CD11b at lower concentration as shown by flow
709 cytometry. E) OXS000275 upregulated CD11b in a dose dependent manner with an EC₅₀ of 238 ± 52
710 nM. F) At 4 days post treatment with OXS000275 a reduced viability and cell number was observed.
711 G) Cytospin preparations of OX000275-treated or PMA-treated HL-60 cells stained with Wright-
712 Giemsa showed signs of myeloid maturation.

713 **Figure 2: Confirmation of HL-60 Differentiation by Global Gene Expression Analysis.** Cells were
714 treated for 3 days with 10 nM of PMA, 1 µM of OXS000275 or 0.1% DMSO. A) Volcano plot of
715 differentially expressed genes between DMSO control and PMA (top panel) and OXS000275. B) Venn
716 diagram of differentially expressed genes post PMA and OXS000275 treatment. C) Heatmap of
717 differentially expressed genes. D) Bulk RNA-sequencing of primary Hematopoietic cells from each
718 population: PCA of each primary Hematopoietic cell population using the top 300 most varied
719 expressed genes: HL-60 cells treated with vehicle (DMSO), PMA or OXS000275 projected onto plot.
720 E) Treatment with OXS000275 and PMA lead to up regulation of genes consistent with myeloid
721 differentiation when assessed by EnrichR and ARCHS4 Tissues signatures. P values were calculated
722 using Fisher exact test, and Enrichment score as enrichment score = $\log(p) \cdot z$, where z is the z-score
723 computed by assessing the deviation from the expected rank. F) Treatment with OXS000275 and
724 PMA lead to gene-expression changes consistent with myeloid differentiation by gene set
725 enrichment analysis.

726 **Figure 3: Development of lead compounds.** A) Lead compounds OXS007417 **2** and OXS007464 **3**
727 were developed from original hits. B) Lead compounds up-regulated CD11b in HL-60 cells by flow
728 cytometry. C) Cytospin preparations of lead compound-treated HL-60 cells stained with Wright-
729 Giemsa showed signs of myeloid maturation.

730 **Figure 4: Lead Compounds Demonstrate Anti-leukemia Activity *In Vivo* in Subcutaneous Xenograft
731 Model and Increased Survival in Orthotropic Model.** A) Experimental outline of HL-60 subcutaneous
732 xenograft model. B) Experimental outline of orthotropic model. C) HL-60 cells were implanted
733 subcutaneously onto the flank of female NOD SCID mice, and the mice were treated with vehicle or
734 indicated compounds; treatment with OXS007417 and OXS007464 reduced tumour growth. D)
735 Example of excised tumours at termination of study; scale bar = 10 mm. E) OXS007417 prolonged
736 the survival in an orthotropic HL-60 model.

737 **Figure 5: Elucidation of Lead Compounds Mechanisms of Action.** A) BioMAP analysis of OXS007417
738 and OXS007464. Primary cell systems created from pooled donors were treated at four indicated
739 concentrations. Cell system specific readouts were taken at time points optimised for each cell
740 system. Readings from treated samples were divided by the average of control readings to generate
741 a ration that was the log₁₀ transformed. Significance prediction envelopes (grey) were calculated
742 from control data at 95% confidence intervals. B) Volcano plot of differentially expressed between
743 DMSO control and PMA (top panel), OXS007417 and OXS007464. C) Venn diagram of differentially
744 expressed genes post PMA, OXS007417 and OXS007464 treatment. D) Heatmap of differentially
745 expressed genes in six biological replicates treated with either OXS007417, OXS007464, PMA (as a
746 positive control for differentiation) or DMSO (solvent only control). E) Treatment with OXS007417

747 and OXS007464 lead to gene-expression changes consistent with myeloid differentiation by gene set
748 enrichment analysis.

749 **Figure 6: Target identification using chemical probe and chemoproteomics** A) Chemical structures
750 of probe **4** and OXS008255 **5**. EC₅₀ values for CD11b upregulation are represented as means ± SEM.
751 In-gel fluorescence showing: B) dose-dependent labelling by probe **4**; C) competition of OXS008255 **5**
752 and paclitaxel with probe **4**; D) competition of inactive analogue OXS007564 **6** with probe **4**.
753 Coomassie stain shows equal protein loading on each gel. Uncropped gels are available in the
754 supplementary information. Volcano plots showing significantly enriched proteins in the pull-down
755 experiment by probe **4** compared to competition with: E) 1 μM of OXS008255 **5**; F) 5 μM of
756 OXS008255 **5**; G) 25 μM of OXS008255 **5**; H) 25 μM of paclitaxel. Full list of proteins for each volcano
757 plot is available in the supplementary information; I) Confirmation of tubulin beta chain enrichment
758 by pull-down and immunoblotting.

759 **Figure 7: OXS007417 causes mitotic arrest via tubulin disruption in HL-60 cells.** A) OXS007417
760 disrupts tubulin polymerisation in a cell free assay. B) Analysis of DNA content by flow cytometry
761 demonstrates G2M arrest in OXS007417 treated HL-60 cells. C) PH3-staining confirms metaphase
762 arrest upon treatment with OXS007417. D) Immunohistochemistry for tubulin (red) and counter
763 staining for DAPI demonstrates spindle disruption by OXS007417.

764

765 **Tables**

Cell Line	Disease	Age	Gender	Source	Molec. Genetics
HL-60	AML M2	35	F	PB	MYC amplification
THP-1	AML M5	1	M	PB	MLL-AF9
KG-1	AML	59	M	BM	Complex Karyotype
OCI AML3	AML M4	57	M	PB	DNMT3A

766 Table 1: Cell line properties

767

Group	n	Treatment	Dose Level	Dosing Route	Dosing Regimen	Formulation	Dose volume
1	10	Vehicle	--	PO	BID	5% DMSO and 95% PBS + 0.1% Tween 20	10 ml / kg
2	10	AraC	20 mg/kg	IP	QD	sterile water	10 ml / kg
3	10	ATRA	5 mg/kg	PO	5 on/2 off	ethanol 10%; CMC-NA 90%	10 ml / kg
4	10	OXS007417	10 mg/kg	PO	BID	5% DMSO and 95% PBS + 0.1% Tween 20	10 ml / kg
5	10	OXS007464	3 mg/kg	PO	BID	5% DMSO and 95% PBS + 0.1% Tween 20	10 ml / kg

768 Table 2: Treatment regimens for subcutaneous model

769

Dose	Database match	BioMap Z-standard	Pearson's Score	# of common biomarkers	Mechanism Class
800 nM	Colchicine 1.1 μ M	17.479	0.896	148	Microtubule Disruptor
	Fosbretabulin Disodium 1.1 μ M	17.247	8.892	148	Microtubule Disruptor
	Fosbretabulin Disodium 3.3 μ M	17.157	0.891	148	Microtubule Disruptor
200 nM	Fosbretabulin Disodium 3.3 μ M	19.495	0.924	148	Microtubule Disruptor
	Fosbretabulin Disodium 10 μ M	19.257	0.922	147	Microtubule Disruptor
	Fosbretabulin Disodium 30 μ M	19.188	0.921	148	Microtubule Disruptor
50 nM	GSK46136A, 370nM	16.977	0.877	148	PLK1 inhibitor
	Vincristine Sulfate, 14 nM	16.926	0.877	148	Microtubule Disruptor
	Pironectin, 14 nM	16.486	0.881	146	Microtubule Disruptor
12 nM	Erastin, 370nM	5.678	0.496	112	VDAC2 Blocker
	SR-2640, 30 μ M	4.851	0.392	140	Leukotriene
	Bemegride, 32 μ M	4.364	0.428	94	GABA-A Receptor Antagonist

770 Table 3: Top 3 similarity matches from an unsupervised search of the BioMAP Reference Database of
771 > 4,000 agents for each concentration of OXS007464. The similarity between agents is determined
772 using a combinatorial approach that accounts for the characteristics of BioMAP profiles by filtering
773 (Tanimoto metric) and ranking (BioMAP Z-Standard) the Pearson's correlation coefficient between
774 two profiles. Profiles are identified as having mechanistically relevant similarity if the Pearson's
775 correlation coefficient is ≥ 0.7 .

776

777

778

Dose	Database match	BioMap Z-standard	Pearson's Score	# of common biomarkers	Mechanism Class
800 nM	Pironetin, 14 nM	18.362	0.911	146	Microtubule Disruptor
	Pironetin, 41 nM	17.424	0.897	146	Microtubule Disruptor
	Epothilone B, 37 nM	17.402	0.895	148	Microtubule Disruptor
200 nM	Pironetin, 14 nM	21.666	0.948	146	Microtubule Disruptor
	Epothilone B, 37 nM	20.508	0.936	148	Microtubule Disruptor
	Epothilone B, 12 nM	19.731	0.927	148	Microtubule Disruptor
50 nM	Paroxetine Hydrochloride, 14 μ M	7.380	0.639	98	SERT Antagonist
	Nifedipine, 14 μ M	6.934	0.612	98	L-type Ca ⁺⁺ Channel Antagonist
	TMP-153, 370 μ M	6.926	0.519	148	ACAT Inhibitor
12 nM	Droperidol, 14 nM	4.935	0.388	148	Dopamine R Antagonist
	Fludrortisone, 14 nM	4.739	0.376	147	GR Agonist
	Sunitinib Malate, 14nM	4.577	0.363	148	VEGFR2 Inhibitor

779 Table 4: Top 3 similarity matches from an unsupervised search of the BioMAP Reference Database of
780 > 4,000 agents for each concentration of OXS007417. The similarity between agents is determined
781 using a combinatorial approach that accounts for the characteristics of BioMAP profiles by filtering
782 (Tanimoto metric) and ranking (BioMAP Z-Standard) the Pearson's correlation coefficient between
783 two profiles. Profiles are identified as having mechanistically relevant similarity if the Pearson's
784 correlation coefficient is ≥ 0.7 .

785

786

787

RANK	PMA			OXS007417			OXS007464		
	Perturbation	1-cos(α)	Cell line	Perturbation	1-cos(α)	Cell Line	Perturbation	1-cos(α)	Cell Line
1	Ingenol 3, 20-dibenzoate	0.6076	PL12	CYT997	0.5679	PL21	CYT997	0.5625	PL2
2	PMA	0.632	PL12	PX12	0.5868	PL21	PX12	0.5773	PL2
3	Ingenol 3, 20-dibenzoate	0.6407	SKM1	LY-2183240	0.5929	THP1	LY-2183240	0.5866	THP1
4	PMA	0.6433	NOMO1	CYT997	0.5981	THP1	CYT997	0.5982	THP1
5	PX12	0.6581	PL21	ABT-751	0.6034	PL21	ABT-751	0.5993	PL21
6	Ingenol 3, 20-dibenzoate	0.6613	HA1E	LY-2183240	0.613	PL21	LY-2183240	0.603	PL21
7	PMA	0.6658	HA1E	PX12	0.6152	THP1	PX12	0.6161	THP1
8	PMA	0.675	SW60	SB225002	0.6159	THP1	ABT-751	0.6199	THP1
9	BRD-k9114395	0.6828	MCF7	ABT-751	0.6192	THP1	SB-225002	0.6249	THP1
10	Ingenol 3, 20-dibenzoate	0.6847	SW60	CYT997	0.6274	SKM1	CYT997	0.6298	SKM1
11	CYT997	0.6848	PL21	ABT-751	0.6333	NOMO1	PMA	0.6346	SW620
12	PMA	0.6865	A375	PMA	0.6391	SW620	Ingenol 3, 20-dibenzoate	0.6366	SW620
13	Ingenol 3, 20-dibenzoate	0.6881	MDST8	SB225002	0.6395	PL21	ABT-751	0.6379	NOMO1
14	PX12	0.6885	THP1	Ingenol 3, 20-dibenzoate	0.6436	SW620	BRD-K92317137	0.6394	THP1

788 Table 5: Top 14 similarity matches in L1000CDS² data base of 6 h RNA-seq signatures.

789

790

Fig. 1

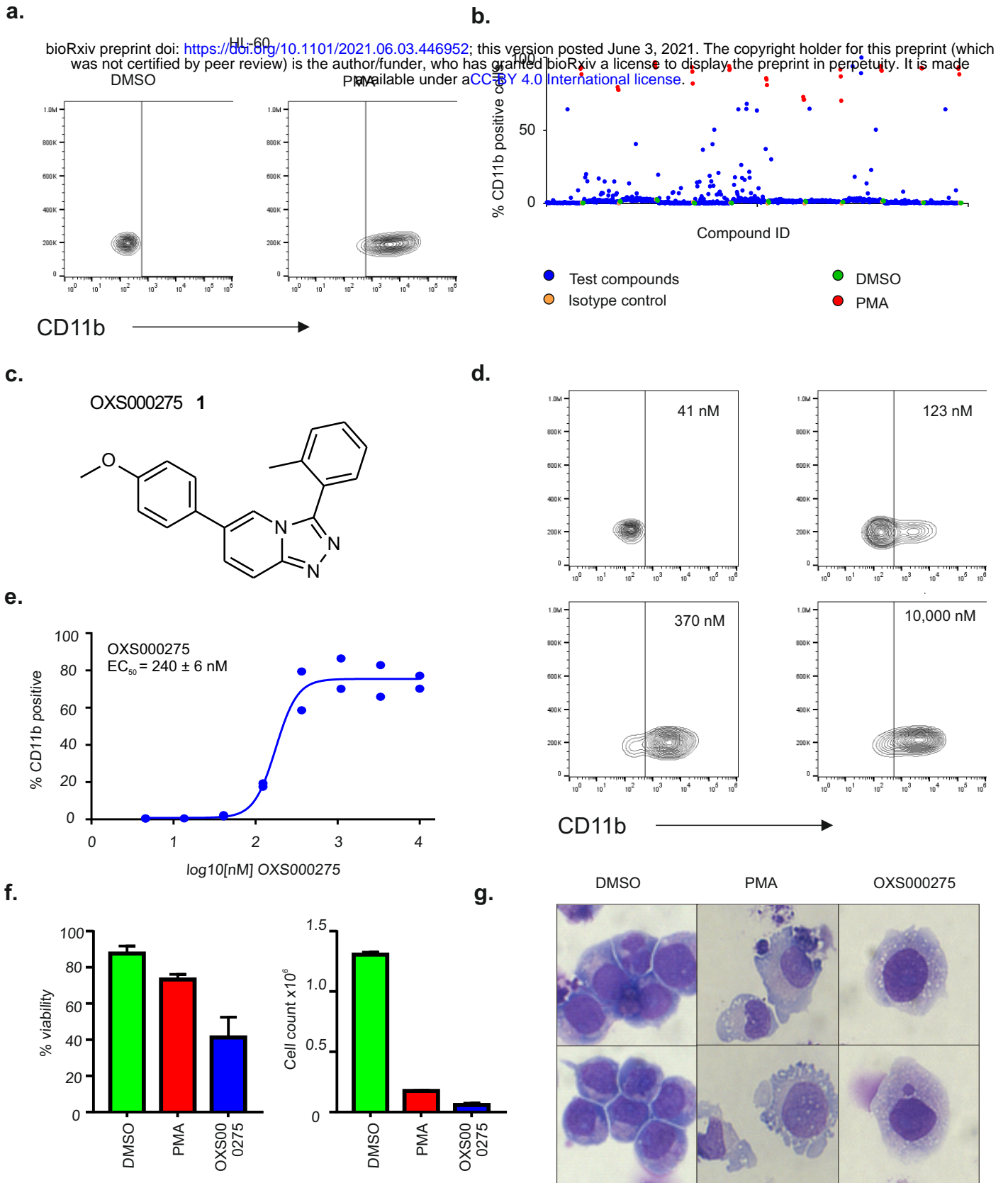


Fig. 2

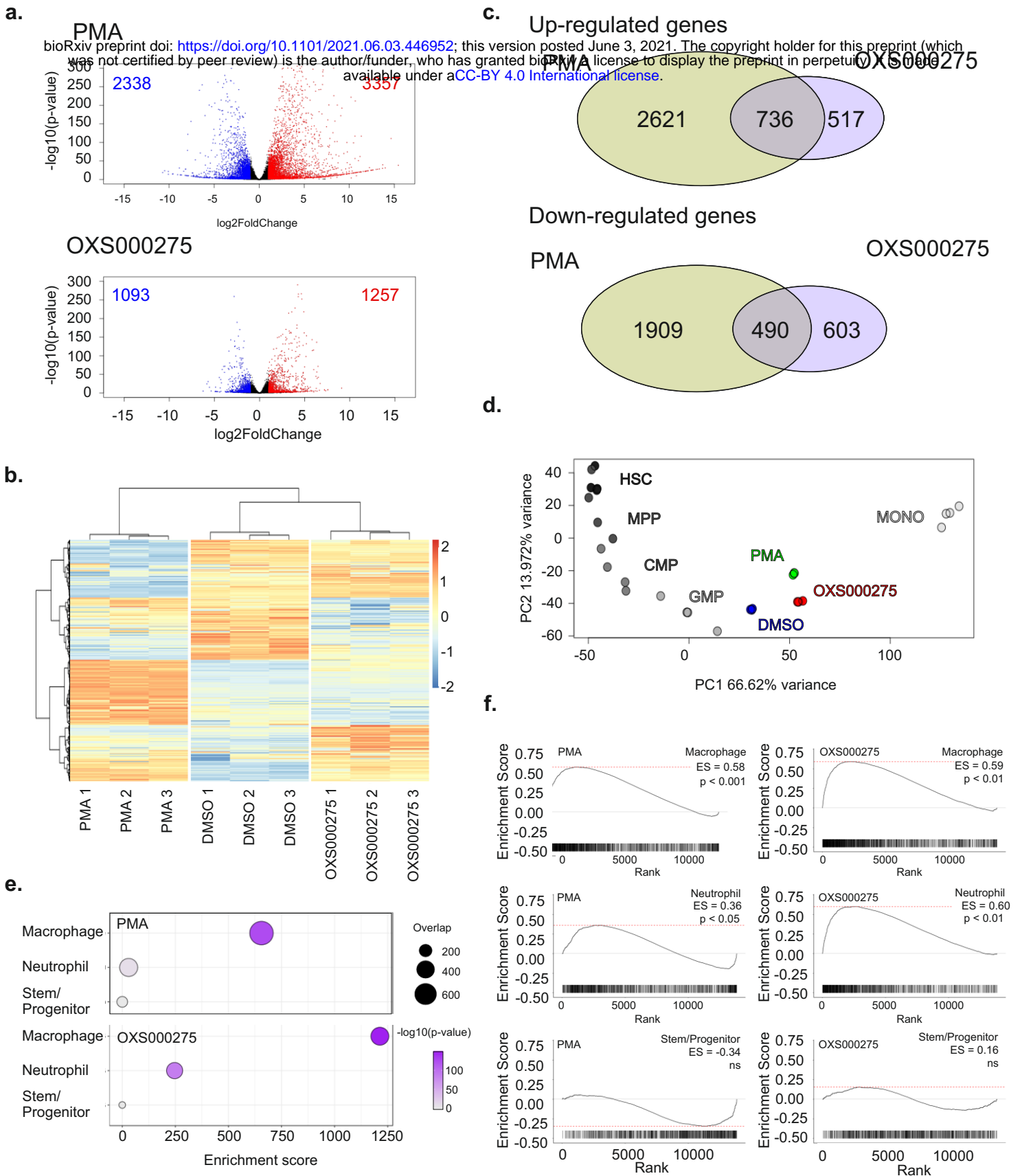
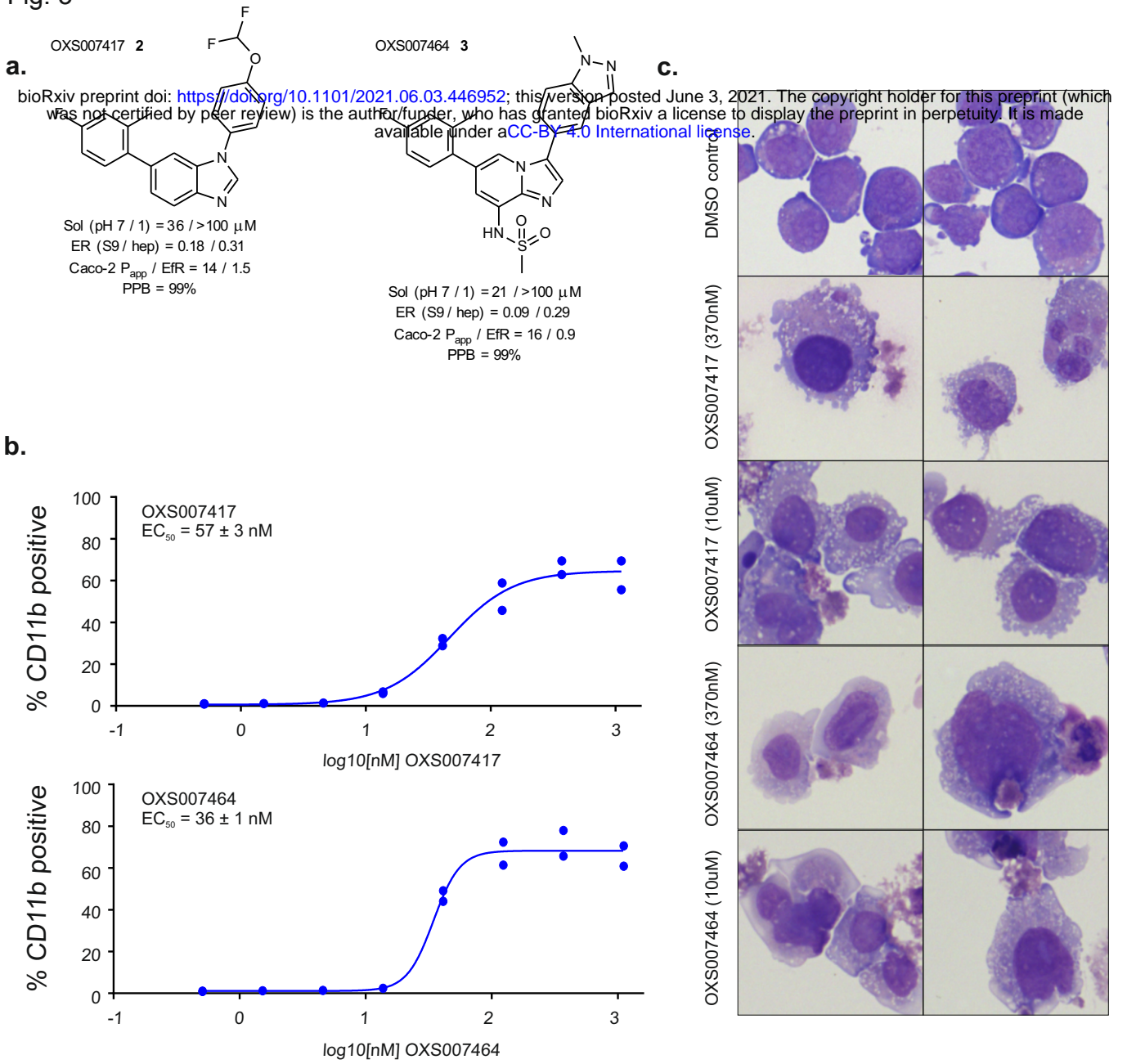


Fig. 3

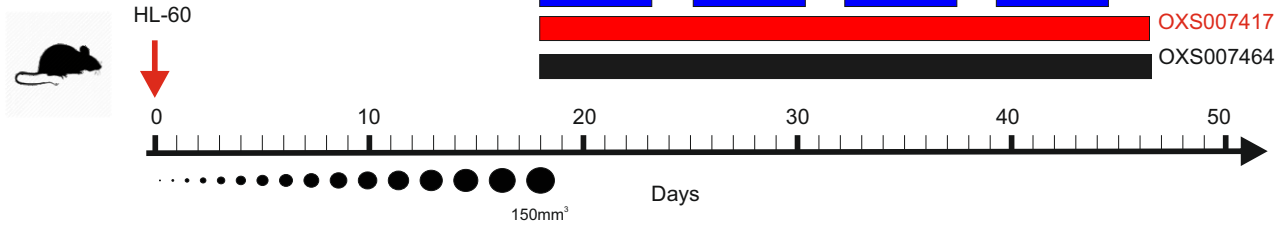


bioRxiv preprint doi: <https://doi.org/10.1101/2021.06.03.446952>; this version posted June 3, 2021. The copyright holder for this preprint (which was not certified by peer review) is the author/funder, who has granted bioRxiv a license to display the preprint in perpetuity. It is made available under aCC-BY 4.0 International license.

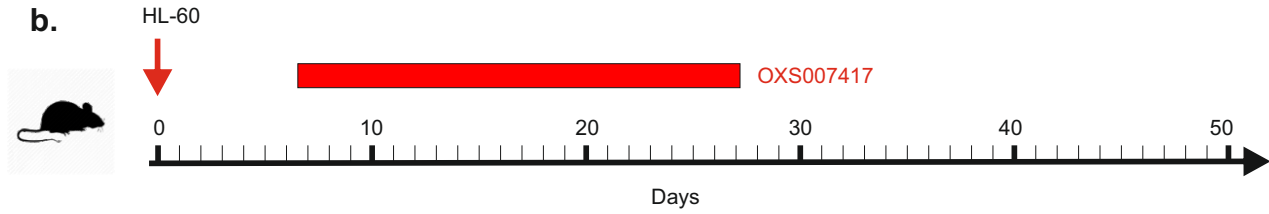
Fig. 4

a.

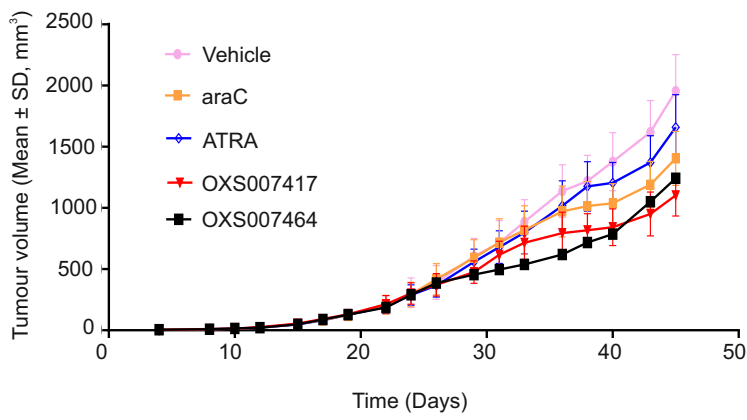
bioRxiv preprint doi: <https://doi.org/10.1101/2021.06.03.446952>; this version posted June 3, 2021. The copyright holder for this preprint (which was not certified by peer review) is the author/funder, who has granted bioRxiv a license to display the preprint in perpetuity. It is made available under aCC-BY 4.0 International license.



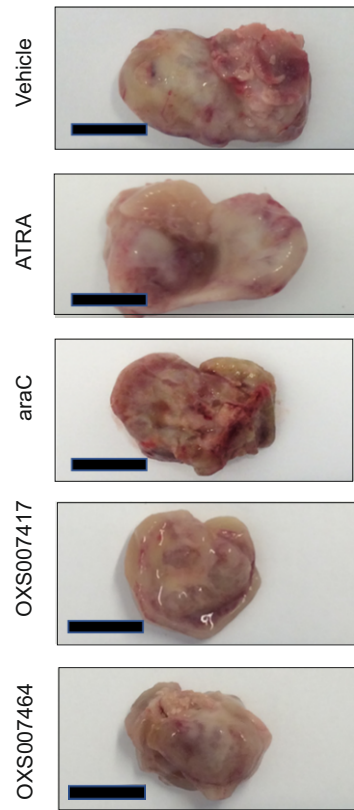
b.



c.



d.



e.

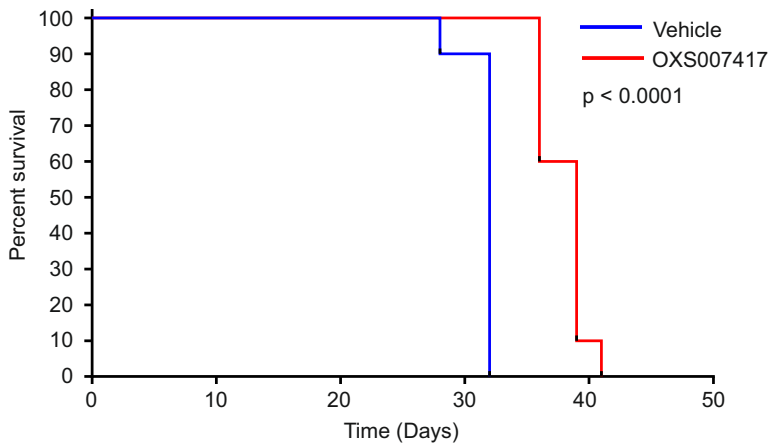


Fig. 5

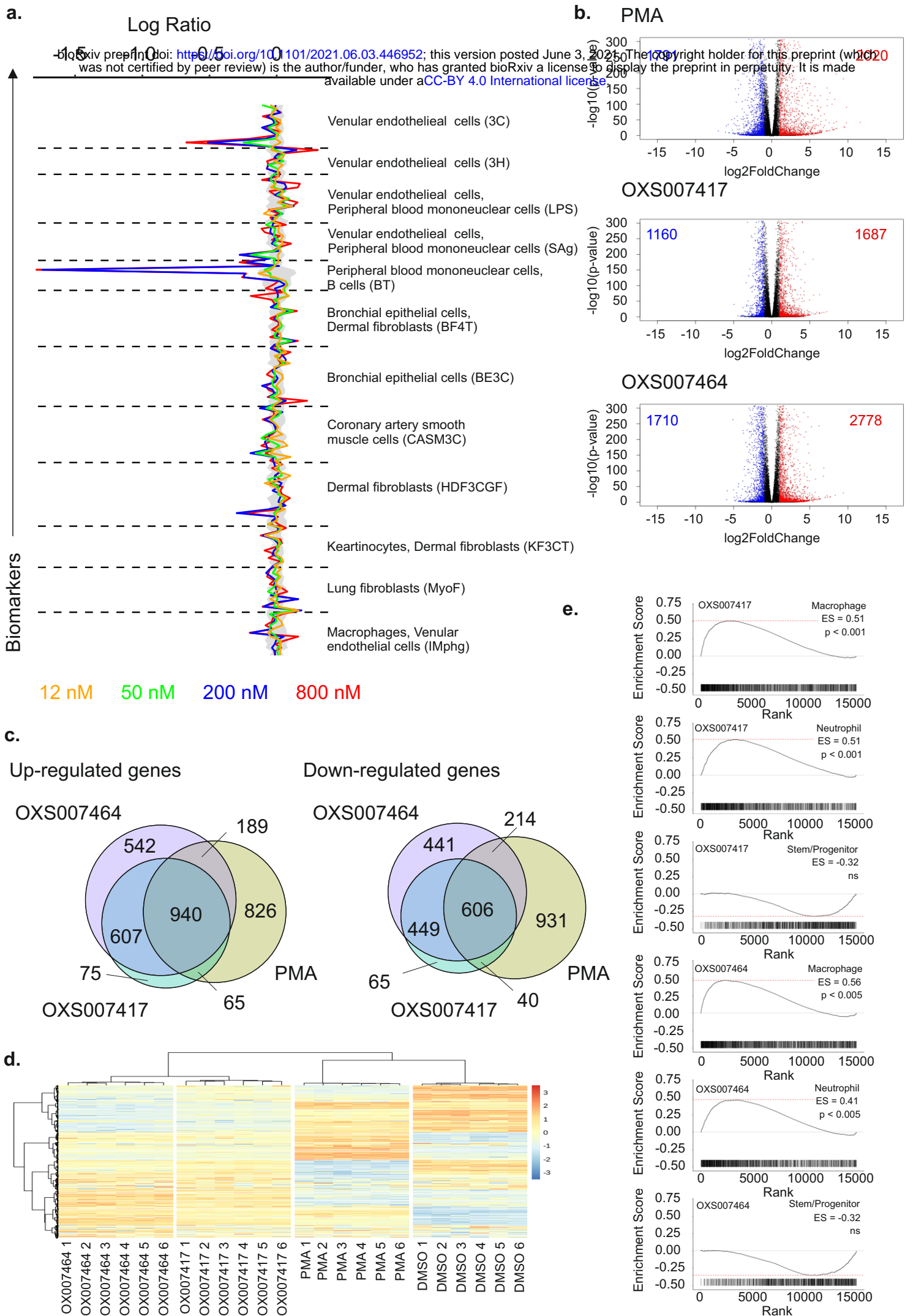
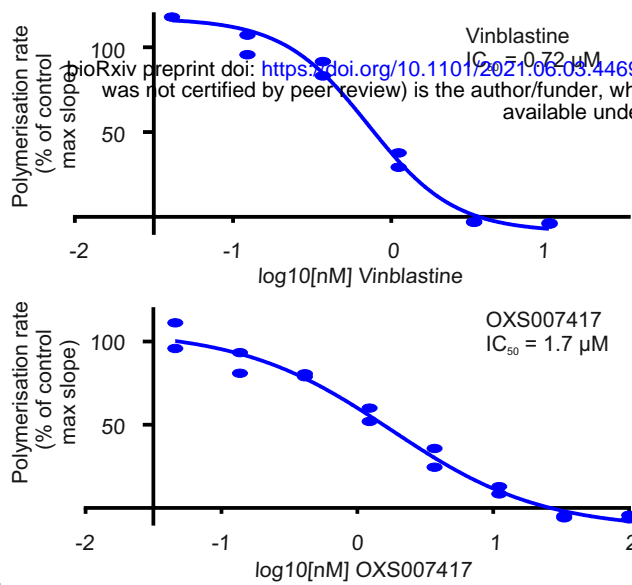
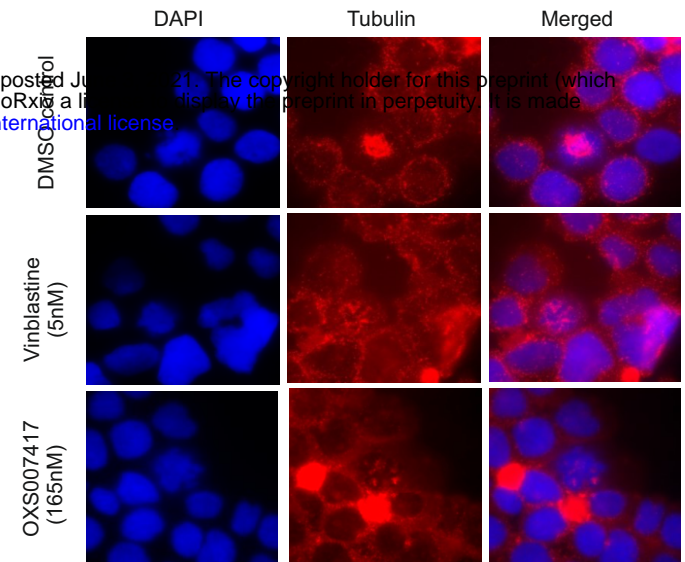


Fig. 7

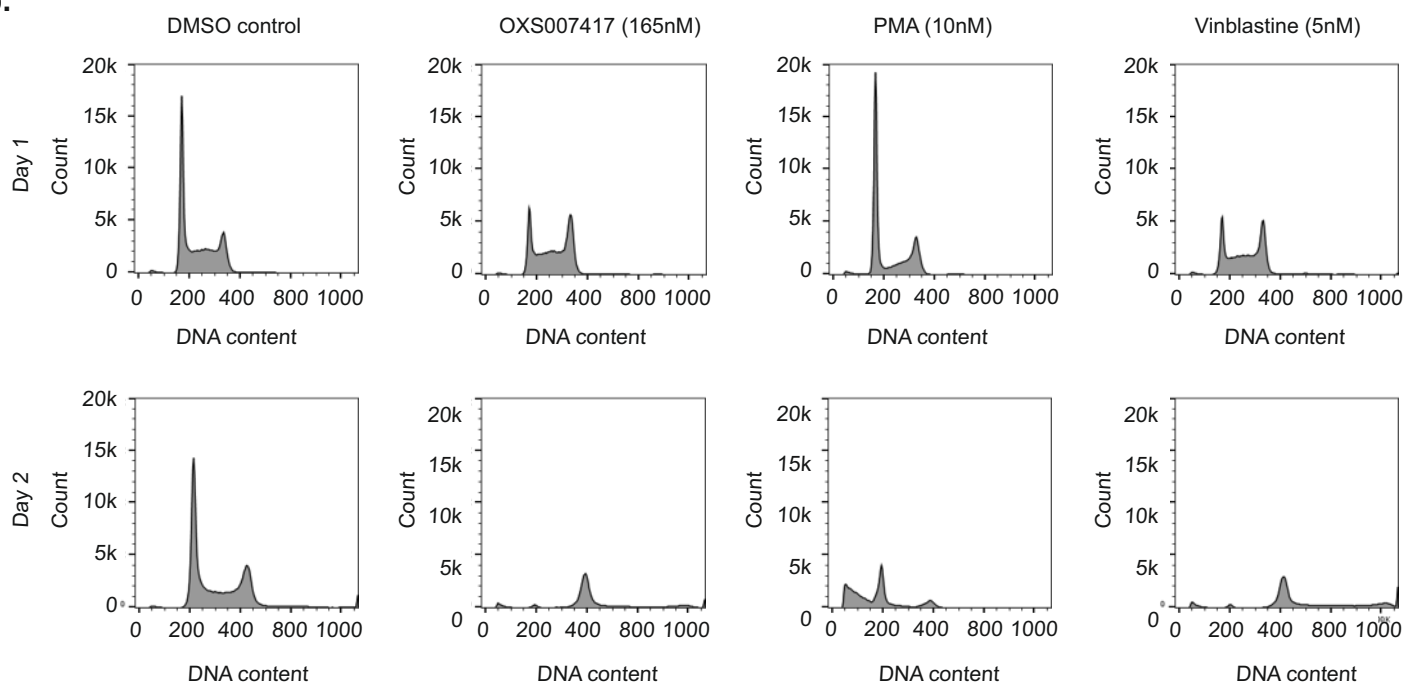
a.



d.



b.



c.

